

Altimetry-derived tide model for improved tide and water level forecasting along the European continental shelf

Hart-Davis, Michael G.; Laan, Stendert; Schwatke, Christian; Backeberg, Björn; Dettmering, Denise; Zijl, Firmijn; Verlaan, Martin; Passaro, Marcello; Seitz, Florian

DOI

[10.1007/s10236-023-01560-0](https://doi.org/10.1007/s10236-023-01560-0)

Publication date

2023

Document Version

Final published version

Published in

Ocean Dynamics

Citation (APA)

Hart-Davis, M. G., Laan, S., Schwatke, C., Backeberg, B., Dettmering, D., Zijl, F., Verlaan, M., Passaro, M., & Seitz, F. (2023). Altimetry-derived tide model for improved tide and water level forecasting along the European continental shelf. *Ocean Dynamics*, 73(8), 475-491. <https://doi.org/10.1007/s10236-023-01560-0>

Important note

To cite this publication, please use the final published version (if applicable).
Please check the document version above.

Copyright

Other than for strictly personal use, it is not permitted to download, forward or distribute the text or part of it, without the consent of the author(s) and/or copyright holder(s), unless the work is under an open content license such as Creative Commons.

Takedown policy

Please contact us and provide details if you believe this document breaches copyrights.
We will remove access to the work immediately and investigate your claim.



Altimetry-derived tide model for improved tide and water level forecasting along the European continental shelf

Michael G. Hart-Davis¹ · Stendert Laan² · Christian Schwatke¹ · Björn Backeberg^{2,3} · Denise Dettmering¹ · Firmijn Zijl² · Martin Verlaan^{2,4} · Marcello Passaro¹ · Florian Seitz¹

Received: 9 February 2023 / Accepted: 30 May 2023 / Published online: 22 July 2023
© The Author(s) 2023

Abstract

With the continued rise in global mean sea level, operational predictions of tidal height and total water levels have become crucial for accurate estimations and understanding of sea level processes. The Dutch Continental Shelf Model in Delft3D Flexible Mesh (DCSM-FM) is developed at Deltares to operationally estimate the total water levels to help trigger early warning systems to mitigate against these extreme events. In this study, a regional version of the Empirical Ocean Tide model for the Northwest European Continental Sea (EOT-NECS) is developed with the aim to apply better tidal forcing along the boundary of the regional DCSM-FM. EOT-NECS is developed at DGFI-TUM by using 30 years of multi-mission along-track satellite altimetry to derive tidal constituents which are estimated both empirically and semi-empirically. Compared to the global model, EOT20, EOT-NECS showed a reduction in the root-square-sum error for the eight major tidal constituents of 0.68 cm compared to in situ tide gauges. When applying constituents from EOT-NECS at the boundaries of DCSM-FM, an overall improvement of 0.29 cm was seen in the root-mean-square error of tidal height estimations made by DCSM-FM, with some regions exceeding a 1 cm improvement. Furthermore, of the fourteen constituents tested, eleven showed a reduction of RMS when included at the boundary of DCSM-FM from EOT-NECS. The results demonstrate the importance of using the appropriate tide model(s) as boundary forcings, and in this study, the use of EOT-NECS has a positive impact on the total water level estimations made in the northwest European continental seas.

Keywords Ocean tides · Numerical modelling · Sea level · Satellite altimetry · EOT

1 Introduction

The ocean is influenced by a variety of physical processes which create complex circulation structures and variable sea surface patterns. One of these processes is the motion caused by the gravitational interaction between the Earth, Sun and Moon called ocean tides. Ocean tides are a significant contributor to the circulation and water levels of the global ocean. In the coastal regions, events that cause episodic rises in

the sea level, such as storm surges, can be further exacerbated when coinciding with high oceanic tides and can therefore increase the likelihood of coastal flooding (Muis et al. 2016). For this reason, alongside having high importance for geodetic and altimetric applications, tides should be carefully considered to improve our understanding of the ocean surface and the implications of short- and long-term sea level rise events (Arns et al. 2017; Intergovernmental Panel on Climate Change 2022).

The theory of ocean tides is well-known due to the relative simplicity and predictability of its forcing (Egbert and Ray 2017). The development of the harmonic method (Darwin 1891) allowed for the decomposition of ocean tides into a finite number of harmonic constants or constituents which can be estimated and combined to provide predictions of the full tidal signal (Pugh 1987; Cartwright 1999). In practice, models of ocean tides do not provide full estimations of the hundreds of tidal constants due to the computational effort as well as the complexity of modelling these constituents. However, the majority of the ocean tide signal can be derived,

✉ Michael G. Hart-Davis
michael.hart-davis@tum.de

¹ Deutsches Geodätisches Forschungsinstitut, Technische Universität München (DGFI-TUM), Munich, Germany

² Deltares, Delft, Netherlands

³ Nansen Environmental and Remote Sensing Center, Bergen, Norway

⁴ Delft Institute of Applied Mathematics, TU Delft, Delft, Netherlands

in most regions, from a small number of these constants termed the major tidal constituents. A study by Egbert and Ray (2017) demonstrates that 99% of the total tidal variance can be captured by fourteen harmonic constants and 99.99% of the variance by eighty constants. This demonstrates the importance of accurately estimating these major tidal constituents to reduce the overall error in ocean tide prediction. However, accounting for the additional smaller constituents, either through direct estimations or inferences using linear admittance, remains crucial for the full tidal estimations (Hart-Davis et al. 2021b).

Although tides have been studied and observed for hundreds of years, advances in our understanding are continuing to take place (Woodworth et al. 2021). This is largely due to the availability of satellite altimetry which allows for a larger spatial observation of the global sea surface than what can be provided by in situ measurements obtained, for example, from tide gauges. The TOPEX/Poseidon (TP) and Jason (JA) series of satellite altimeters have provided a consistent sampling on a tide-favourable orbit for 30 years, which has allowed for ocean tides in the open ocean to be well studied during this period (for example, Provost et al. 1995; Andersen 1995; Egbert and Ray 2003; Savcenko and Bosch 2012; Hart-Davis et al. 2021a). Additionally, data from the Envisat-ERS-Saral altimeters have provided a large temporal dataset on a constant orbit that is different to that of the TP-JA orbit. When these data are combined and used in empirical models, there has been an overall improvement in the tidal estimations (Hart-Davis et al. 2021a).

Recent developments in tidal modelling have continued to improve our understanding of global ocean tides (Lyard et al. 2021). Although the estimation of open ocean tides is relatively reliable, largely thanks to the previously mentioned availability of satellite altimetry, weaknesses continue to remain in the coastal and shelf regions (Stammer et al. 2014). Land contamination of satellite altimetry data nearer to the coast and poorly resolved bathymetry products are key culprits to these weaknesses, not to mention the complexity of tides in the coastal regions. Satellite altimetry-derived empirical ocean tide models benefit from developments made in the field of coastal altimetry, with clear evidence being shown in two recent publications (Cheng and Andersen 2017; Hart-Davis et al. 2021a), with the latter demonstrating the importance of the retrieval of data closer to the coast, made possible by the use of the ALES retracker (Passaro et al. 2014). As these tide models continue to improve, they become more valuable as corrections within coastal altimetry applications, but these improvements serve several different applications. One such application is the use of these tide models as boundary forcings for operational ocean models, which rely on tide models to account for the tidal influence which is crucial in terms of improving the model accuracy.

One such operational model is a series of hydrodynamic models for the Northwest European Shelf developed for the Dutch Directorate-General for Public Works and Water Management (Rijkswaterstaat) (Goede 2020). The latest model, the Dutch Continental Shelf Model in Delft3D Flexible Mesh (DCSM-FM), has been developed using the state-of-the-art unstructured hydrodynamic modelling software Delft3D Flexible Mesh Suite (Zijl and Groenenboom 2019; Kernkamp et al. 2011). Previous generation models were specifically aimed at operational forecasting of water levels under daily storm surge conditions and were schematized as depth-averaged 2D tide-surge models (Zijl et al. 2013, 2015). This latest generation model has been proven to be suitable for a wider range of applications such as water quality and ecology studies, oil spill modelling, search and rescue and providing three-dimensional boundary conditions of salinity and temperature for detailed models. The high value of water level forecasting within DCSM-FM underlines the importance of providing appropriate tidal boundary forcings, which play a significant role in determining the accuracy of the model.

The aims of this manuscript are two-fold: the first is to develop a regional high-resolution version of an empirical ocean tide model that improves on the global configuration with respect to in situ measurements and provides additional tidal constituents previously not included. The second aim is to apply this improved regional tide model to the hydrodynamic model DCSM-FM at the boundaries to improve the model's estimation of the tidal height and total water levels with respect to in situ measurements along the northwest European continental shelf. The manuscript is structured as follows: a detailed description of the developed regional Empirical Ocean Tide for the North European Continental Shelf (EOT-NECS) model, as well as the presentation of an updated tide gauge dataset (TICON-3), is presented in Section 2. The EOT-NECS model is then validated against these tide gauges and, where appropriate, is contrasted to both EOT20 and the FES2014 tide models in Section 3. In Section 4, DCSM-FM is described before several experiments are presented and evaluated that aim at improving the models' tidal height and total water level estimations. Finally, a conclusion is made based on both of the aims mentioned above, and potential further developments which would benefit DCSM-FM are discussed.

2 Data and methodology

2.1 EOT-NECS

The EOT20 model provided a valuable global ocean tide product that has proved to be useful for the field of satellite

altimetry, particularly in its use in the tidal correction (Hart-Davis et al. 2021a). Through the continued use of the model as well as user feedback, several avenues were identified that would benefit the accuracy of the model. The most obvious initial addition to the Empirical Ocean Tide (EOT) model configuration is the inclusion of several additional satellite altimetry missions. These altimeter datasets are the Sentinel-3A (S3A), Sentinel-3B (S3B), Saral (SA), Saral drifting phase (SDP) and Sentinel-6A (S6A) missions, the latter being the latest extension of the long-standing TP-JA orbit (an overview of the missions used and their respective time-period is provided in Fig. 1). There is additional value in the inclusion of the SA altimeter which continues the orbit of the ERS-Envisat (ER-EN) missions also previously included in EOT20; however, due to the sun-synchronous orbit of these missions, also for S3A and S3B, these orbits cannot be used alone to derive a full estimation of the ocean tides.

The additional altimetry missions provide new orbits into the model (Fig. 2), which are appropriate for optimising the weighted sea-level anomaly (SLA) estimations for each node of the EOT configuration. Using these data, two EOT models are created: (1) a purely empirical model made out of only satellite altimetry data and uses no reference tide model to correct the SLA data and (2) a residual tide model based on using the FES2014 as a tidal correction for the SLA data. These two models follow the same methodology described in Hart-Davis et al. (2021a). The SLA data were obtained from along-track altimetry by applying the altimetry corrections listed in Table 2 of Hart-Davis et al. (2021a). Additionally, the model configuration was refined to more accurately deal with the instrument error from the altimetry observations and improve the outlier detection to allow for more reliable input data used in the tidal analysis. These two refinements are important points to account for the difficulties of sea level retrieval from satellite altimetry (Cipollini et al. 2017). These were identified as points of improvement in EOT20 since it is

clear that when not appropriately accounted for, outliers and errors in SLA data will negatively influence the amplitude and phase determinations of tidal constituents. As described in Savcenko and Bosch (2012) and Hart-Davis et al. (2021a), a variance component estimation (VCE) is also conducted within EOT to allow for the combination of different missions by weighting each mission based on their variances calculated for each node using an iterative process. In addition, all the missions used were cross-calibrated and adjusted to each other by applying radial corrections (Bosch et al. 2014).

Once completed, the tidal analysis is conducted on the resultant SLA observations to estimate the harmonic constants of individual constituents of interest. Due to the resultant tidal estimation being the sum of the ocean and load tide contributions, known as the elastic tide, a final step to separate the ocean and load tide contributions is done following the technique presented in Cartwright and Ray (1991); Savcenko and Bosch (2012); Hart-Davis et al. (2021a), with only the ocean tide component being of interest for the rest of this study.

The models are gridded onto a 1/16 degree spatial resolution, which is an increased spatial resolution relative to the global EOT20 model (1/8 degree). A total of 42 constituents for both model versions are estimated. These constituents were chosen based on the requirements of the work presented later in this publication; however, these tides were also within the capabilities of the altimetry data used to make the tidal estimations. The two model versions allowed all constituents available in the reference tide model, FES2014, to be taken and additional constituents not contained within the FES2014 atlas to be estimated as purely empirical estimations. This combined residual and empirical set of constituents resulted in the Empirical Ocean Tide model for the Northwest European Continental Sea (EOT-NECS). The list of constituents used is the same as those presented in Section 4.

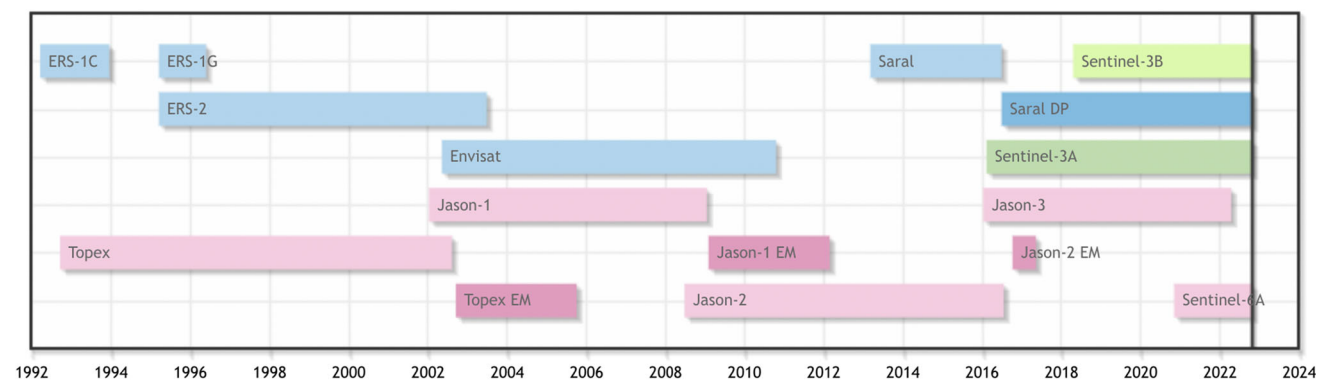


Fig. 1 The satellite altimetry data used in EOT-NECS, taken from OpenADB (<https://openadb.dgfi.tum.de/en/>). The missions presented with the same colours are those that follow the same orbit. Note for the final

version of EOT-NECS data up until 2022-10-31 is used, indicated by the black vertical black line within the plot

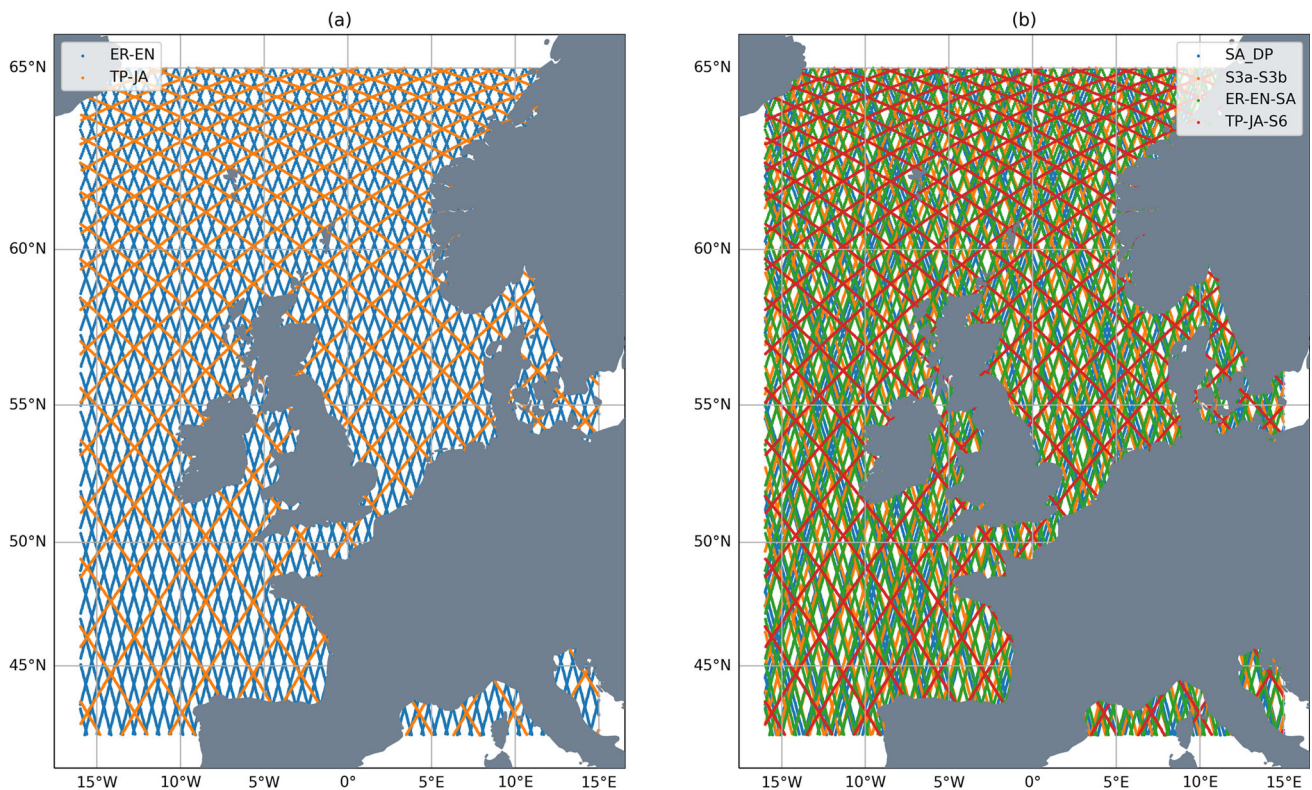


Fig. 2 The spatial coverage of the altimetry data used in the (a) EOT20 and (b) EOT-NECS tide models

Limitations can be placed on the estimation of certain tides if the orbit of the satellites are not able to properly resolve certain tidal constituents. The ER-EN-SA and the S3A/S3B orbit missions, for example, are not able to make estimations of the solar tides (S1, S2, etc) based on their sun-synchronous orbits. The aliasing period, the length of data required to estimate individual constituents based on the respective orbits of the missions, is also important to consider when including altimetry missions which have been providing data for a relatively short period. All 42 constituents can be safely estimated following the Rayleigh criteria following the technique presented in Smith (1999) with the resultant calculations shown in Fig. 11 in the Appendix.

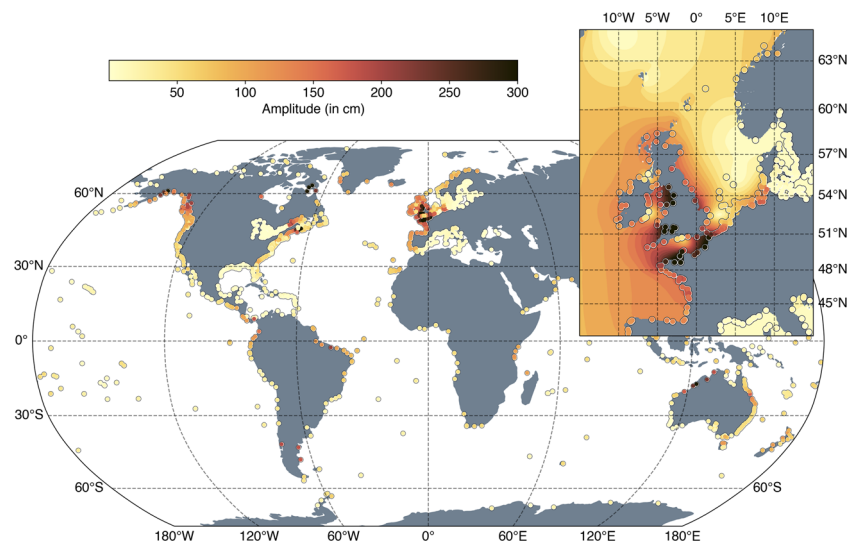
2.2 Tide gauge validation dataset

Tide gauges provide valuable data for the validation of ocean tide models. Using the GESLA-2 tide gauge dataset, a dataset of Tidal CONstants (TICON) was produced in Piccioni et al. (2019). In late 2021, an update to the GESLA dataset called GESLA-3 was produced which quadrupled the number of globally available tide gauges (Haigh et al. 2022). Based on this, an update to TICON, termed TICON-3, was done, which increased the number of tide gauges and maintained the same 40 constituents included in the previous version

of the dataset (Hart-Davis et al. 2022a). A total of 3471 tide gauges are now available within the TICON-3 dataset, with additional information being included from the provided GESLA-3 files about whether the tide gauge is a coastal, lake or river tide gauge. Figure 3 demonstrates the global distribution of TICON-3 and the subset in the north European shelf used to validate the developments of EOT-NECS model.

Although the GESLA-3 updated dataset includes 5119 tide gauges, several of these have a relatively short time series (less than 1 year) which does not meet the requirements of data required in the TICON processing to have at least 1 year of continuous data. Furthermore, there are several duplicated tide gauges which is a result of obtaining data from multiple data sources. In TICON-3, these gauges remain within the dataset to allow users themselves to distinguish which data sources they would like to use. In this study, duplicated tide gauges are removed from the analysis to reduce impacts on the estimated mean statistics. Additionally, for some of the minor tides estimated, not all tide gauges may be appropriate based on the length of available time series. Again, these data remain within the TICON-3 dataset; however, care should be taken when interpreting the resultant estimations for these minor tides. In this study, when validating the minor tidal constituents, only gauges with at least 5 years' worth of data are used to account for potential errors that may occur in shorter time series.

Fig. 3 The global distribution of tide gauges within the TICON-3 dataset, with a subplot shown to demonstrate the tide gauges used to validate EOT-NECS. The coloured dots represent the M2 amplitudes estimated at the individual tide gauges, while the background plot shows the M2 amplitude from EOT-NECS



3 Validation of EOT-NECS

The TICON-3 dataset, which contains 389 tide gauges in the domain of interest (Fig. 3), is used to validate the results of the developed EOT-NECS compared to both FES2014 and EOT20 (Fig. 4). Here, the root-mean-square error (RMS) for constituents and the root-square-sum error (RSS) for the eight major tides are compared, following the techniques presented in Stammer et al. (2014) which uses the modelled amplitude (A_m) and phase (p_m) and the observed amplitude (A_o) and phase (p_o) for each constituent to determine the RMS as follows:

$$RMS = \sqrt{(A_o \cdot \cos(p_o) - A_m \cdot \cos(p_m))^2 + (A_o \cdot \sin(p_o) - A_m \cdot \sin(p_m))^2}, \tag{1}$$

and then the RSS is estimated for each tide gauge based on the RMS of the eight major tides.

$$RSS = \sqrt{\sum RMS_{[M_2, S_2, K_1, K_2, N_2, P_1, O_1, Q_1]}}. \tag{2}$$

For each tide gauge, the RSS and RMS were estimated and are presented in both Figs. 4 and 5. For each of the major tides, there is an overall mean improvement in EOT-NECS compared to EOT20 with an average RSS improvement being 0.678 cm, with this being seen in the majority of tide gauges in the domain. This is somewhat expected based on the extension of the TP-JA orbit with the incorporation of additional data from Jason-3 as well as the inclusion of the recent Sentinel-6A. This extension means that the TP-JA orbit is sampled for 30 years allowing for a reliable estimation of the major tidal constituents and the additional estimation of some of the minor tidal constituents. Based on these results,

the extension of the previously used altimetry datasets, the incorporation of new altimetry data and the improved spatial resolution of the model benefit the resultant tidal estimations.

In Fig. 5, the RMS of additional constituents is presented. Tides available in EOT20 continue to improve in the EOT-NECS model except for the SA tide, which showed a slightly degraded RMS. EOT-NECS improves the estimates for all constituents compared to FES2014 besides the NU2 tide, which shows a higher mean RMS. For the constituents where FES2014 does not contain data, these constituents in EOT-NECS were derived from purely empirical estimates and do not benefit from the use of the FES2014 reference model in the coastal region. Several of these constituents, which are minor tidal constituents having small tidal signals compared to the major tides and a small contribution to the overall tidal signal, have relatively high RMS values compared to tide gauges. These tides are difficult to estimate directly from satellite altimetry data based on their small signals compared to the noise of altimetry data retrieval, particularly in the coastal regions. However, these tides are not available in empirical estimations and were sources of errors in DCSM-FM, making them prime candidates for experimental testing later on in this study.

Of particular interest is the inclusion of the MA2 and MB2 constituents which can reach relatively large amplitudes in certain regions both globally and within the region of interest (Ray 2022). To the best of our knowledge, these tides are not available in any global empirical ocean tidal atlases that could be used in this region, at least none that are publicly available, which motivated their incorporation into the EOT-NECS developments and, eventually, within DCSM-FM. The tide gauges in this region indicate a mean tidal amplitude of 1.61 cm and 1.15 cm for the MA2 and MB2 constituents, respectively, reaching up to 10.30 cm and 8.69 cm, respectively. Considering the relatively small amplitudes, the RMS

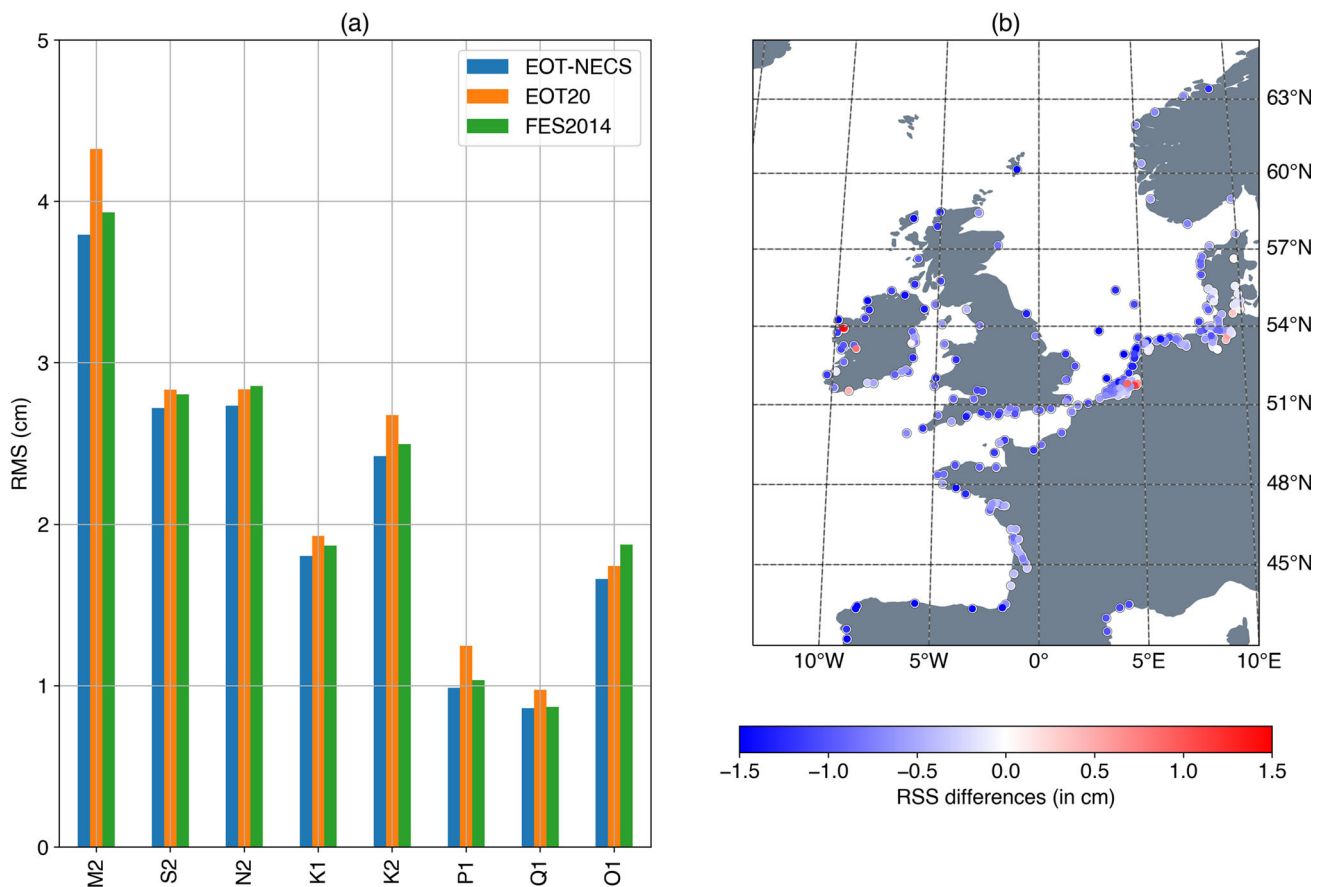


Fig. 4 (a) RMS against 389 tide gauges in the North-West European Coastline of the eight major tidal constituents. (b) RSS difference between EOT20 compared to EOT-NECS. Blue indicates a lower RSS for EOT-NECS, and red indicates a higher RSS

differences of EOT-NECS are relatively high for these two constituents, exceeding 1 cm on average. However, despite this, we expect the open ocean estimation of these tides to be better relative to the coastal region, and therefore, these two tides are still appropriate for testing as a tidal boundary forcing.

In the production of EOT20, a first look at uncertainties was conducted by estimating the variance factor of the model. This so-called variance of unit weight (see Bähr et al. 2007, for example) is determined during the VCE by evaluating the weighted sum of squares of the residuals for each node of the model based on the input altimetry datasets. Based on the results of the VCE, a variance factor can be determined for each node of the model and can be complemented with the tide gauge analysis to evaluate whether the tidal estimations are improving. Although this quantity does not represent the full model uncertainties, due to the absence of uncertainty metrics in FES2014, it provides valuable insights especially to assess performance differences between different model versions when combined with the full in situ tide gauge validation.

It is expected that if the variance factor of EOT-NECS decreases with respect to EOT20, the estimations of EOT-

NECS are improved. To test this, the percentage variance factor difference is estimated following $var_{DIFF} = ((var_{EOT20} - var_{EOT-NECS}) / var_{EOT20}) \cdot 100$, with the results presented in Fig. 6. Throughout the model domain, there is a reduction in uncertainties in the updated model configuration. Larger variance reductions are seen in regions of large tidal ranges, particularly in the Bay of Biscay, the English Channel and the Irish Sea. The variance differences further cement the idea that the changes made to the EOT model have an overall positive impact on the estimation of tides.

4 Using EOT-NECS as boundary forcing of DCSM-FM

4.1 Description of DCSM-FM

The Dutch Continental Shelf Model in Delft3D Flexible Mesh (DCSM-FM) covers the Northwest European Continental Shelf from 15°W to 13°E and 43°N to 64°N. The model has been developed in the Delft3D Flexible Mesh Suite (Kernkamp et al. 2011), which allows for an unstructured grid

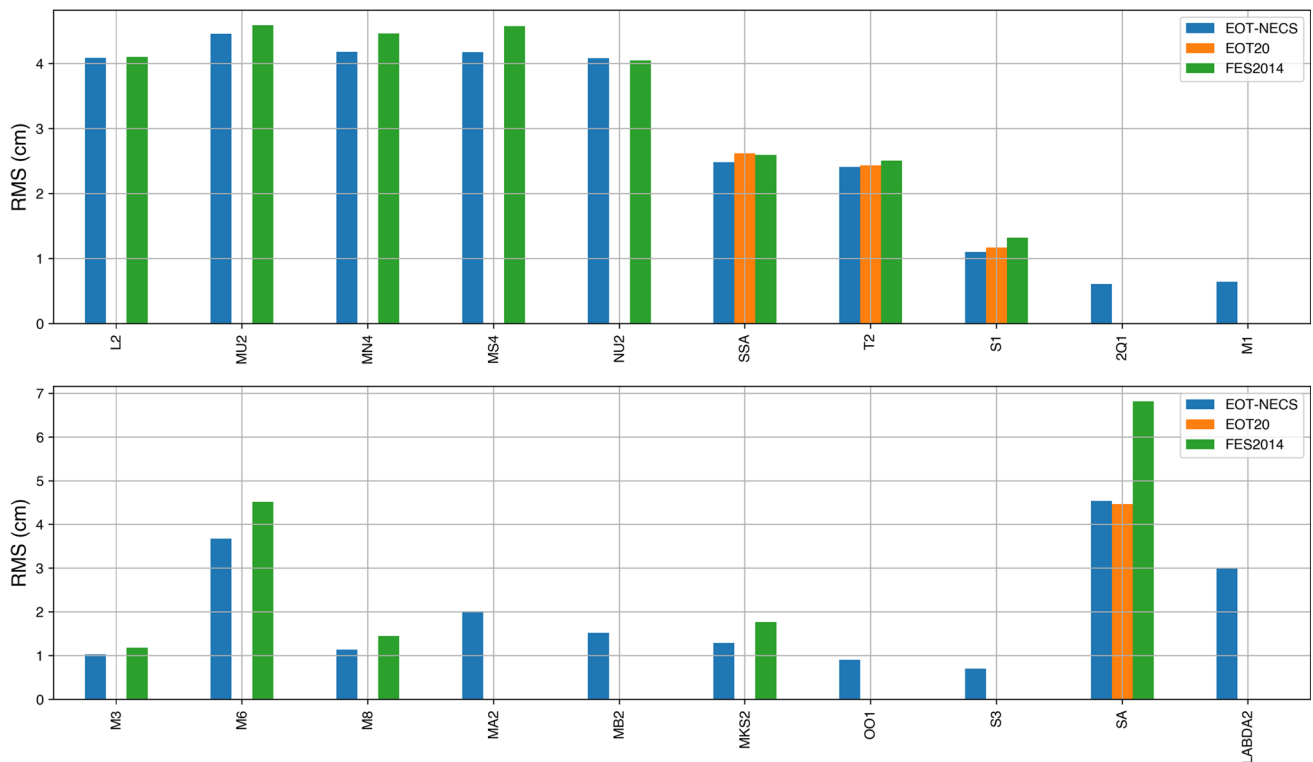


Fig. 5 RMS validation against TICON-3 for additional tidal constituents available from EOT-NECS. The RMS differences, where applicable, are compared to available constituents from EOT20 and FES2014

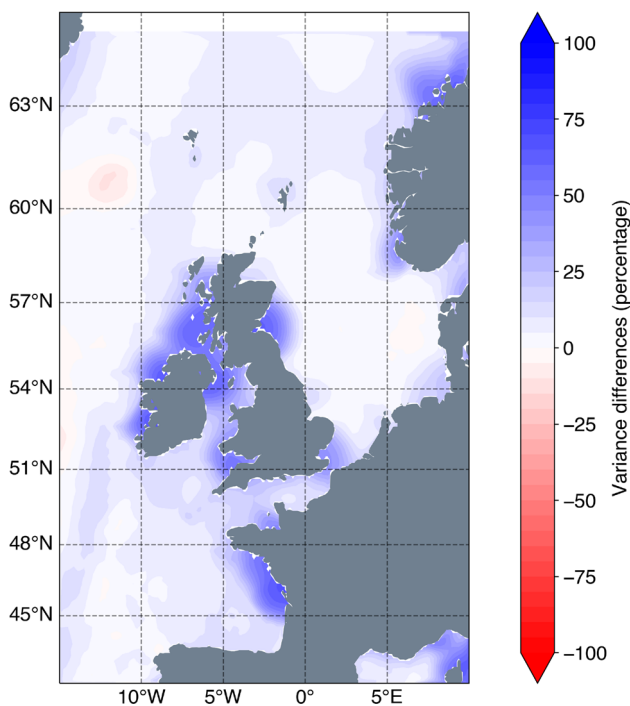


Fig. 6 The percentage variance factor change of EOT-NECS with respect to EOT20 as determined from the VCE described in (Savcenko and Bosch, 2012; Hart-Davis et al., 2021a). A reduction in variance is shown as blue, and an increase is red

approach. The grid of the horizontal schematization has an increasing resolution from 4 nm (nautical miles)/7.408 km in deep oceanic waters to 0.5 nm/0.926 km in shallow coastal waters and the southern North Sea. Refinements with a factor of 2 by 2 are placed at roughly the 800 m, 200 m and 50 m isobaths which ensures the grid cell size scales with the square root of the depth to limit variations in the wave Courant number.

The model bathymetry is derived from the bathymetric data of EMODnet Bathymetry Consortium (<https://www.emodnet-bathymetry.eu>/EMODnet Bathymetry Consortium 2020) and the Dutch Directorate-General for Public Works and Water Management (Rijkswaterstaat). Depths are written to the grid nodes based on the average value of the data within a surrounding area of the size of the corresponding grid cells. Other geometric information, such as dry areas, thin dams and weirs, are based on the World Vector Shoreline (<https://shoreline.noaa.gov/>) and data by Rijkswaterstaat. For the bottom roughness, a spatially varying Manning roughness coefficient is used. The Manning roughness coefficient varies from 0.012 to 0.050 s/m^{1/3}. This value is calibrated for multiple areas within the model domain to obtain an optimal water level representation. The method used is explained in Zijl et al. (2013). For this calibration, simulations with the 2D depth-averaged model were conducted for 2017 to converge

the model results to water level observations at more than 200 tide gauges within the model domain (Zijl et al. 2013).

The spatial forcing of the air-sea momentum flux in the model is taken from the ERA5 reanalysis dataset by ECMWF (Hersbach et al. 2017). For consistency with the atmospheric boundary layer in ERA5, the same temporally and spatially varying Charnock coefficient is used for the air-sea momentum exchange. In the 3D model, additional spatial forcing for the heat flux is included from ERA5. To account for the radiative heat fluxes, the surface net solar (short-wave) radiation and the surface downward long-wave radiation have been imposed, while the surface upward long-wave radiation is computed based on the modelled sea surface temperature. In addition, freshwater discharges at 847 locations are included as monthly mean discharges based on climatology from E-HYPE (Hackett et al. 2013). At the open boundaries, water levels are forced as a combination of different components,

with the amplitude and phases of tidal constituents being included (see Fig. 7 for an illustration of the S1 tide). Currently, these tides have been taken from a combination of the DCSMv6, GTSMv4.1 and FES2014 models (Table 1). Based on the information provide by the models, a tidal water level signal is constructed within Delft3D Flexible Mesh as a combination of simple harmonic constituent motions. To determine this signal, the nodal amplitude factor and astronomical argument are automatically re-calculated every 6h. In addition, tide-generating forces within the model domain are included. These forces are based on the gravitational forces of the terrestrial system on the water mass. Furthermore, an estimation of offshore surge levels is included by the addition of an inverse barometer correction (IBC) based on the local atmospheric pressure. Lastly, a daily mean sea surface height is forced to include the density-driven effects or the mean dynamic topography (MDT) at the boundaries taken

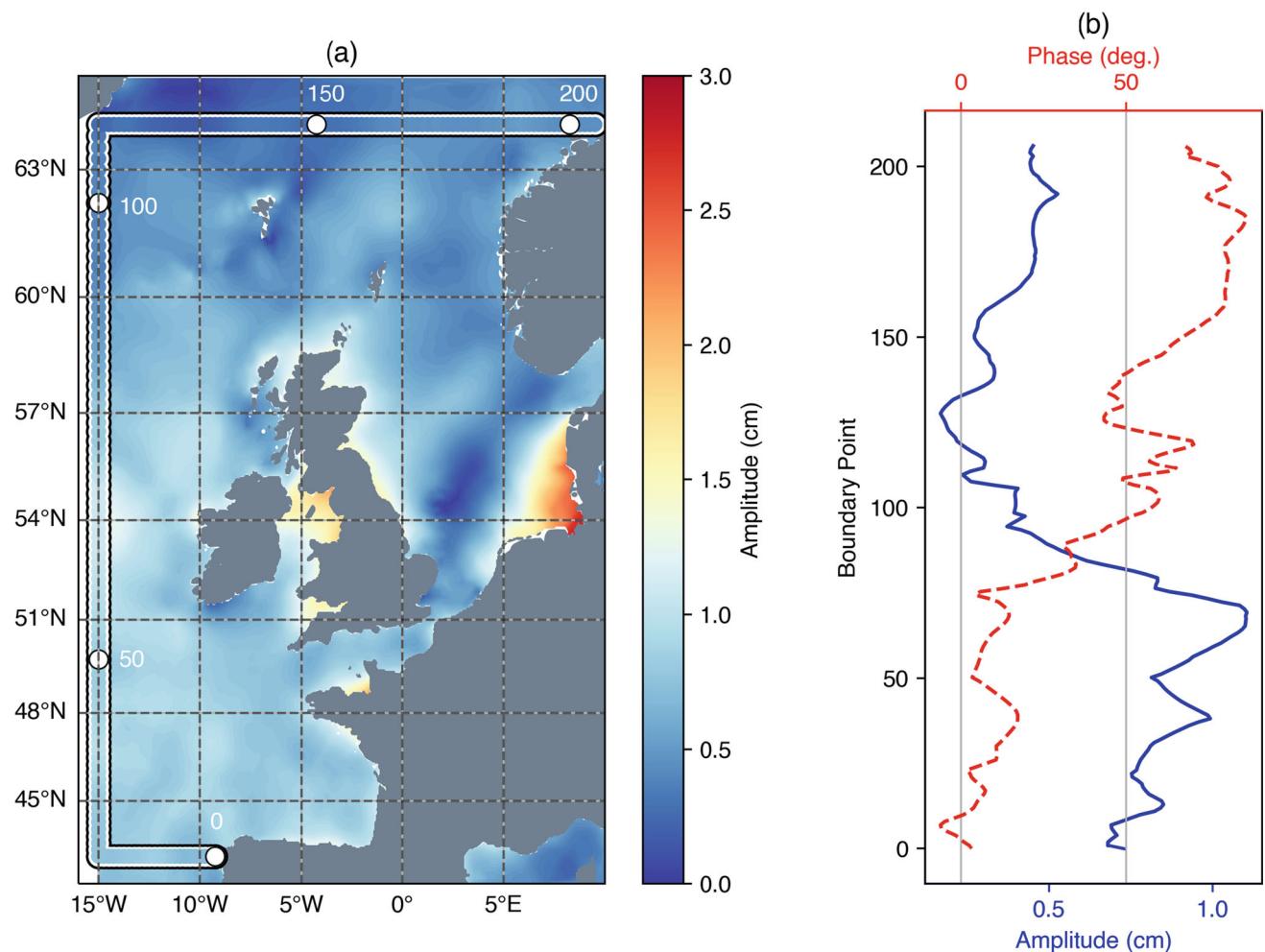


Fig. 7 The position of the lateral boundaries of the DCSM-FM model where the model is tidally forced. In this figure, the background is the EOT-NECS S1 tidal amplitude with the markers indicating the position of the boundary and the associated amplitude. **(b)** demonstrates the

amplitude (cm) and phase (degrees) along the boundary of EOT-NECS. The white dots in **(a)** correspond to the the respective boundary points which are to be used as reference for **(b)**

Table 1 The list of constituents and their associated angular frequency [°/h] used on the boundaries to force DCSM-FM, with original sources taken either from DCSMv6, GTSMv4.1 or FES2014. The column ‘Experiment’ describes the respective experiment where these tides are replaced with those from EOT-NECS. The + is used for the SA tide, which for the 2D model version uses DCSMv6 while the 3D model uses FES2014

Tide	Angular frequency	Source	Experiment
SA	0.041069	DCSMv6 +	3D-DCSM
SSA	0.082137	FES2014	DCSM-D
MM	0.544375	FES2014	
MSF	1.015896	FES2014	
MF	1.098033	FES2014	
MFM	1.642408	FES2014	
MSQM	2.113929	FES2014	
2Q1	12.85429	GTSMv4.1	DCSM-D
SIGMA1	12.92714	GTSMv4.1	
Q1	13.39866	FES2014	
RHO1	13.471515	N/A	DCSM-C
O1	13.94304	FES2014	
NO1	14.49669	GTSMv4.1	
PI1	14.91786	GTSMv4.1	
P1	14.95893	FES2014	
S1	15	FES2014	DCSM-B
K1	15.04107	GTSMv4.1	
LABDA2	15.51259	FES2014	DCSM-D
J1	15.58544	FES2014	
EPSILON2	27.42383	FES2014	
2N2	27.89535	FES2014	
MU2	27.96821	FES2014	DCSM-D
N2	28.43973	GTSMv4.1	
NU2	28.51258	FES2014	DCSM-D
MA2	28.943036	N/A	DCSM-C
M2	28.9841	GTSMv4.1	
MB2	29.025173	N/A	DCSM-C
MKS2	29.06624	FES2014	DCSM-D
L2	29.52848	FES2014	DCSM-D
T2	29.95893	FES2014	DCSM-D
S2	30	FES2014	
R2	30.04107	FES2014	
K2	30.08214	GTSMv4.1	
ETA2	30.62651	GTSMv4.1	
M3	43.47616	GTSMv4.1	
N4	56.87946	FES2014	
MN4	57.42383	GTSMv4.1	
M4	57.96821	FES2014	
MS4	58.9841	GTSMv4.1	
S4	60	FES2014	
M6	86.95231	FES2014	DCSM-D
M8	115.9364	FES2014	DCSM-D

from the reanalysis dataset with the GLORYS model (<https://doi.org/10.48670/moi-00021>) as provided by the Copernicus Marine Environment Monitoring Service (CMEMS). Also, three-dimensional daily mean salinity, temperature and advection velocity data from the same source are forced at the open boundaries. In the 2D depth-averaged model, these last three forcings are not directly forced but indirectly included by spatially forcing the difference between the multiyear mean water level field computed by a 2D and 3D version of this model.

4.2 The impact of EOT-NECS on the 2D DCSM-FM

To evaluate the importance of including certain individual tidal constituents at the boundary forcings of DCSM-FM, several versions of the 2D configuration were run. These experiments assess the impacts of adding individual or groups of constituents on the overall accuracy of the model. Each of the 2D model simulations was run for a total of 5 years from 1st January 2013 to 1st January 2018, with the resultant estimated individual constituents and the total tidal heights and total water levels being the subject of evaluation within this study. The selection of which constituents to include in the experiments was based on the previous DCSM-FM versions which identified these constituents as being highly erroneous or constituents that were not previously available from other model estimations. Three model simulations are compared to a reference simulation of DCSM-FM (DCSM-A), which contains the constituents listed in Table 1, except for the MA2, MB2 and RHO1 constituents which were previously not forced at the boundary. The original ‘Source’ of constituents is described within Table 1.

The experiments are as follows: (A) being the reference run; (B) the S1 constituent from EOT-NECS is used; (C) the previously not included MA2, MB2 and RHO1 constituents are added from the EOT-NECS model; and (D) constituents that were previously available from other tide models are replaced by the EOT-NECS model constituents based on their relative accuracy compared to in situ tide gauge valuations (a breakdown of the constituents is given in the ‘Experiment’ column of Table 1). The experiments are designed to build on the previous experiment, as constituents continue to be used in the following experiments, i.e. DCSM-C also uses the S1 tide from EOT-NECS used in DCSM-B, and DCSM-D uses those from the DCSM-C experiment.

The first experiment was to test the impact of the S1 tidal constituent from the EOT-NECS model compared to using the FES2014 S1 tide on the accuracy of the model relative to tide gauges (Fig. 8A). This model version is termed DCSM-B. At the boundaries, the S1 tidal constituent showed relatively large differences between EOT20 and FES2014 and, within the reference simulation of DCSM-A, showed

high RMS values for both amplitude and phase compared to in situ tide gauges. Along the boundary of DCSM-FM, the mean difference between the amplitude and phase of EOT20 and FES2014 is 0.25 cm and 5.31° respectively. When including the S1 tide from EOT-NECS, the predicted S1 improves with respect to tide gauges (Fig. 8I). This improvement is particularly strong along the Dutch coastline, with the RMS reducing by 3.16 mm relative to the tide gauges in this region, with the rest of the domain having a reduction of 1.52 mm. Considering that the S1 tidal signals at these tide gauges (estimated following Stammer et al. 2014) are 7.19 mm, this is a median improvement of 28.10% and 43.95% overall and along the Dutch coastline, respectively.

The replacement of the S1 tide within DCSM-B does not have a major influence on other tides, no constituent changes by more than 1%. The RSS was estimated from all the tidal constituents that were forced at the boundary as

seen in Table 1, except for the MA2, MB2 and RHO1 constituents which were previously not used to force DCSM-A. The mean RSS reduction relative to DCSM-A of the MA2, MB2 and RHO1 constituents (Fig. 8E) was 1.91 mm. More importantly, when assessing the influence that the S1 tide has on the tidal and water height levels estimated by DCSM-B, a mean RMS reduction of 2.21 mm and 1.73 mm was seen, respectively. This reduction in RMS in the DCSM-B tidal and water level estimations is consistent throughout the entire domain of DCSM-FM.

Based on being identified as highly erroneous constituents within the DCSM-A simulation results, the second experiment (DCSM-C) involved three additional tides from EOT-NECS which were previously not included in the boundary forcing of DCSM-FM: MA2, MB2 and RHO1. It is important to emphasise that these constituents have been added to the constituents used in the DCSM-B experiment, i.e. S1

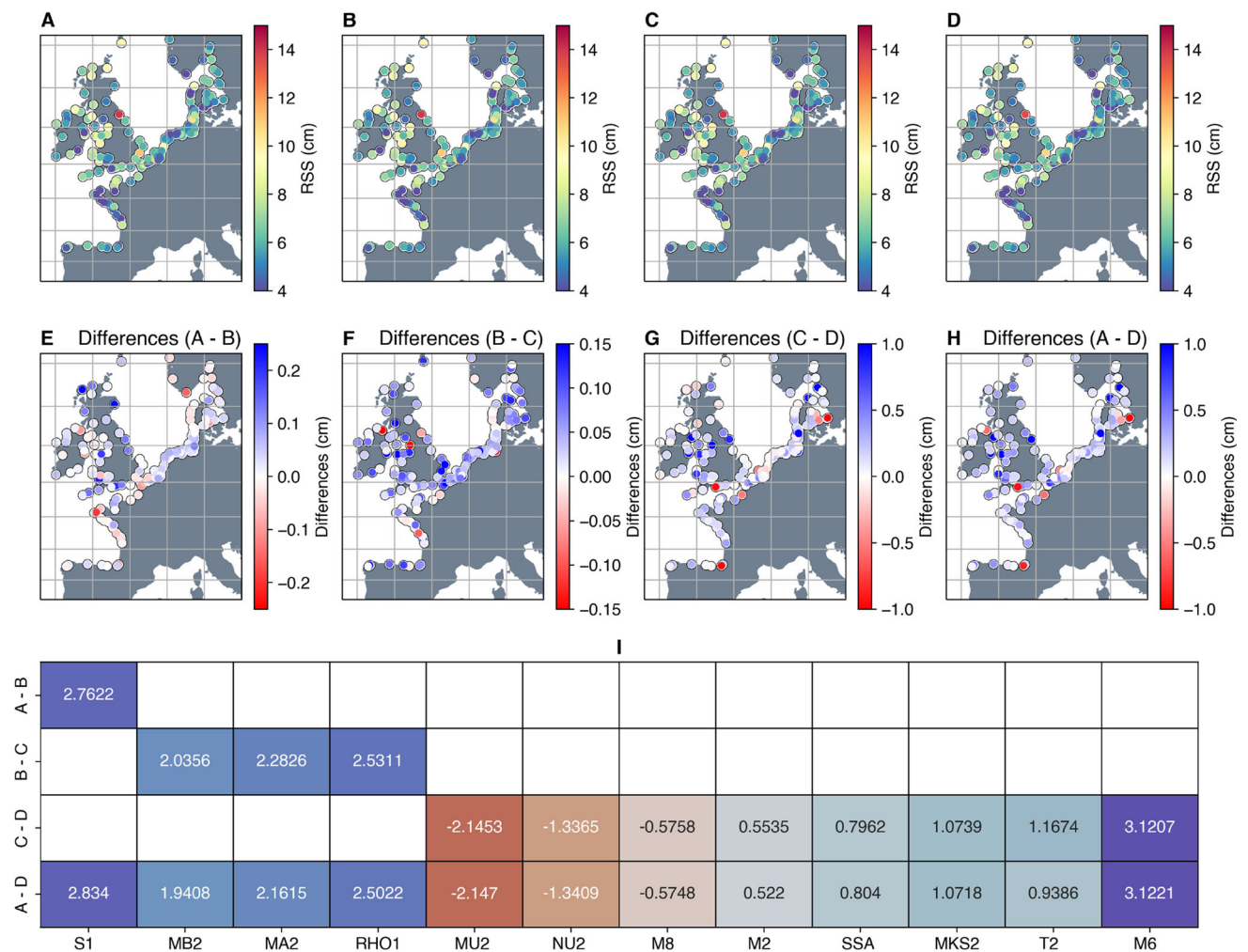


Fig. 8 The RSS of all the constituents tested in each version of DCSM-FM. A to D represent the different DCSM-FM experiments, while E to H describe the differences between the versions. I presents a table

of the RMS differences (in mm) between the different experiments of individual constituents, with only constituents with an absolute RMS difference of more than 0.5 mm shown

from EOT-NECS is also used, and therefore, results will be contrasted to the results of DCSM-B and not DCSM-A. In DCSM-A, these tides demonstrated high RMS errors for these constituents of 5.80 cm and 1.61 cm respectively while RHO1 has an RMS error of 0.31 cm.

In this region, the maximum tidal signal estimated by EOT-NECS for the MA2, MB2 and RHO1 tides is 1.52 cm, 1.85 cm and 0.86 cm, while the mean tidal signal is 0.23 cm, 0.24 cm and 0.10 cm. In DCSM-C, all three of these tides show an improvement in their estimation with respect to DCSM-B (Fig. 8I). This improvement is consistent throughout the entire domain, with the Irish Sea and the Dutch-German coastlines being the regions with the greatest improvement for all three tides. When considering the tidal signals of these tides, all exceed a 20% improvement, with RHO1 improving by 52%. These results highlight the benefit of incorporating these tides from EOT-NECS at the boundary of DCSM-FM.

When estimating the RSS from all the constituents, DCSM-C has a mean reduction of 0.41 mm relative to DCSM-B, with improvements seen throughout the domain. The estimated total tidal and water height had a reduced RMS in DCSM-C of 0.24 mm and 0.21 mm, respectively. The magnitude of the reductions varies between regions, with the Bay of Biscay and Irish Sea showing a 0.60 mm and 0.39 mm reduction in tidal height RMS and a 0.63 mm and 0.33 mm reduction in total water level RMS, respectively. For the Skagerrak Strait, a negligible increase of 0.03 mm in RMS for both tidal height and total water levels.

The final experiment, DCSM-D, was to switch out some constituents already within DCSM-A with some now available from EOT-NECS. This was decided based on their performance with respect to tide gauges in Fig. 5, their ability to be reliably estimated from satellite altimetry (Fig. 11) as well as being tides where DCSM-A contained a relatively large errors. The chosen ten constituents were, again, added to those from the DCSM-C experiment. Unlike the previous experiments, which all resulted in positive impacts for each of the tides tested, for some tidal constituents, DCSM-D demonstrated a degradation relative to DCSM-C. The biggest two negative impacts were the MU2 and NU2, whose mean RMS values increased (Fig. 8I) consistently throughout the domain. In Hart-Davis et al. (2021b), these two tides were highlighted as tides that were not suitable to be directly estimated from along-track satellite altimetry within the EOT configuration for certain regions. Instead, it is recommended to obtain these tides from linear admittance or from a numerical model. In this study, they were included to provide a different test to those presented in Hart-Davis et al. (2021b). However, from these results as well as those presented in previous studies, it is clear that the MU2 and NU2 tides should not be directly estimated, at least not currently, within the EOT configuration. Instead, either linear admittance (Egbert and Ray 2017; Ray 2017) or a numerical model should be

used to estimate MU2 and NU2, such as in the DCSM-A case where FES2014 was used. The only other tide with significant negative impacts is M8. Relative to this tide's tidal signal, 5.91 mm, an increase in RMS of 9.71% was seen; however, the negative result of this tide is region-dependent. When removing the Skagerrak Strait from the analysis, which accounted for most of the mean RMS increase of 1.58 mm, the RMS differences became negligible.

Mean RMS improvements were seen throughout the domain for the SSA, MKS2, T2 and M6 constituents (Fig. 8I). For the L2 and 2Q1 tides, negligible differences (<0.05 mm) between DCSM-C and DCSM-D were seen. Interestingly, in this simulation, a constituent that was not changed improved, namely the M2 tide. However, these changes relative to the tidal signal in this region, which can exceed 300 cm, should be considered insignificant, despite the positive result. The mean RSS differences between DCSM-C and DCSM-D were also negligible, being below 0.27 mm on average. However, this is predominantly driven by errors in the NU2 and MU2 constituents. As shown in Fig. 8G, despite the influence from MU2 and NU2, there are still certain regions where the RSS is improved. When these two tides are removed from the RSS estimation, there is a mean reduction of 2.03 mm, with this consistent throughout the domain (see Appendix Fig. 12).

For the total tidal and water height, both estimations show an improvement of 0.49 mm and 0.52 mm relative to DCSM-C, respectively. There were larger reductions in RMS in the Dutch and German coastlines, with an average of 0.98 mm in the tidal height and 1.01 mm in total water height in DCSM-D with respect to DCSM-C. As expected, regions where the M8, MU2 and NU2 errors are larger have a negative impact on the tidal and water height estimations. In the Skagerrak Strait, negative differences of 0.50 mm for the tidal height and 0.37 mm for the total water height were seen.

The overall change from DCSM-A to DCSM-D (Fig. 8H) was a 0.85 mm reduction in RSS, with this increasing to 2.61 mm when the MU2 and NU2 tides are removed from consideration. The overall mean improvement made from DCSM-A to DCSM-D based on tidal height and the total water level was 0.29 cm and 0.25 cm, respectively (Fig. 9) based on these experiments, which is a significant improvement made to the tidal estimations particularly based on errors in model derived tidal constituents exceeding 4 cm in the coastal region (Lyard et al. 2021; Hart-Davis et al. 2021a), also shown in Fig. 4. When considering that the mean sea level rise estimated from satellite altimetry in the North Sea is 2.6 mm/year (Dettmering et al. 2021) and errors in tidal estimates are a large contributor to the uncertainty of water level estimates (van de Wal et al. 2019; Prandi et al. 2021), these reductions in the overall error of tidal height and water level estimations within the model are crucial, particularly when considering that these constituents are considered minor tides, having much smaller contributions to the overall tidal height. In

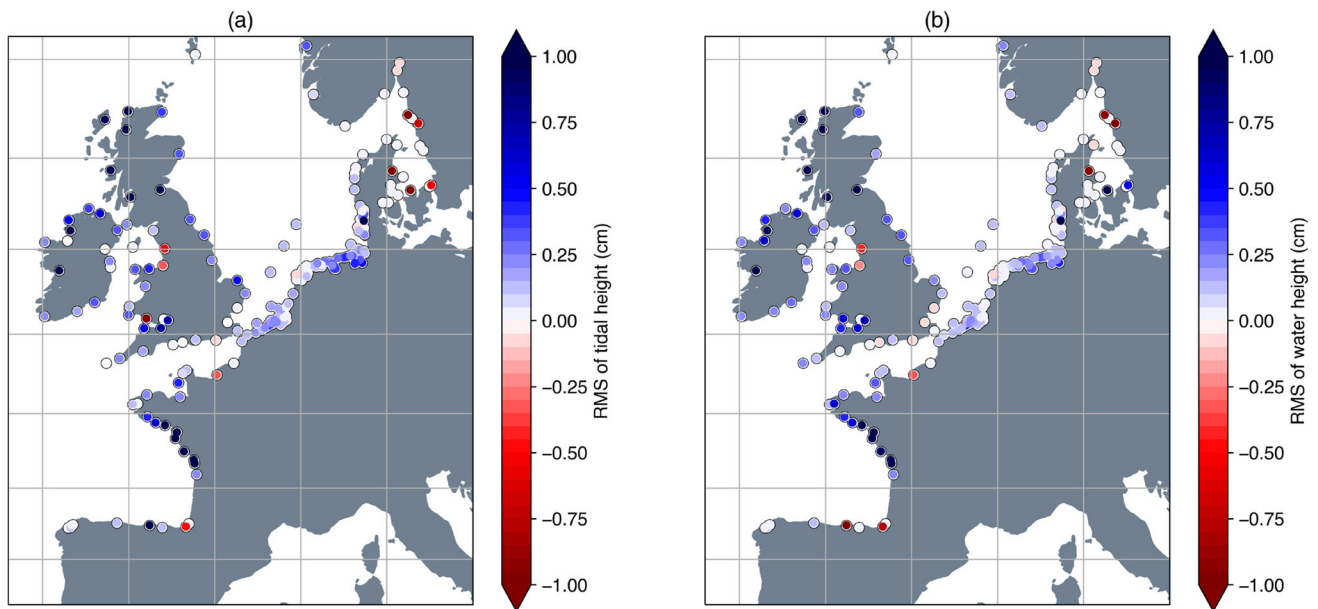


Fig. 9 The overall RMS changes with respect to tide gauge observations in both tidal height (a) and water levels (b) estimations from DCSM-A to DCSM-D. A blue value indicates a higher RMS in DCSM-A, while a red value indicates a higher RMS in DCSM-D

some regions, the overall improvements made to the model in the Bay of Biscay, the English Channel and the Irish Sea even surpass 1 cm (see Fig. 9). These improvements made to DCSM-FM, also along the Dutch coastline which is the main area of application of the 2D model, demonstrate the positive impact of the appropriate tidal forcing on the model's performance.

4.3 The impact of EOT-NECS on the 3D DCSM-FM

To evaluate the influence of these tidal constituents on the 3D version of DCSM-FM, two 3D model versions were run for a 1-year period, from 01 January 2017 to 01 January 2018. The first model version was a reference model (3D-DCSM-REF) that incorporated no tidal constituents from EOT-NECS, while the second model version included all the constituents from EOT-NECS that were used in DCSM-D of the 2D experiments (all the constituents listed mentioned in 'Experiment' in Table 1) as well as the inclusion of the SA tide (3D-DCSM-EOT). The inclusion of the SA tide was based on 3D-DCSM-REF previously using FES2014 to force this tide in the 3D model, recalling that the SA tide was taken from the DCSMv6 in the 2D experiments, and EOT-NECS showing an improvement in this tide with respect to FES2014.

Overall, the differences between the two models were very small, with both the total tidal height and total water level differences being less than 0.005 mm on average. Despite this negligible difference, there are differences in the RMS estimation of the individual constituents. A degradation of the

SA tide of 7.08 mm was seen, while the S1, RHO1, MA2, MB2, M6 and MKS2 tides all showed improved RMSs of more than 0.5 mm when being included from EOT-NECS. The increased RMS of the SA tide causes an increase in the RSS estimation of the 3D-DCSM-EOT version (Fig. 10a). The SA tide from the EOT set of models, i.e. both EOT20 and EOT-NECS, is influenced by non-tidal variability, namely mesoscale and seasonal variability. This results in the tide from EOT not being appropriate for all applications, and based on the results seen in Fig. 10a, this is also the case for this application.

Furthermore, the SA tide is influenced by the dynamic atmospheric correction (DAC), which is used in the derivation of the SLA data used to make the tidal estimations in EOT-NECS. As the boundaries of DCSM-FM incorporates an inverse barometer correction which aims to incorporate signals similar to that estimated in the DAC, it is expected that this SA tide signal is being over-counted, which results in these reductions in accuracy with respect to tide gauges. Additionally, as mentioned previously, the density fields for the 3D model run are taken from the GLORYS ocean model, which will also have a contribution of the SA tide within. Accounting for these two contributions to the SA tide means that this constituent requires special treatment in future iterations of the model and cannot simply be taken as is from EOT-NECS to be used as a boundary forcing within DCSM-FM. Further experiments will take place in follow-up research to determine what the best solution for DCSM-FM is regarding this constituent.

Despite this, there is a clear benefit in including several tidal constituents from EOT-NECS. To demonstrate this, in

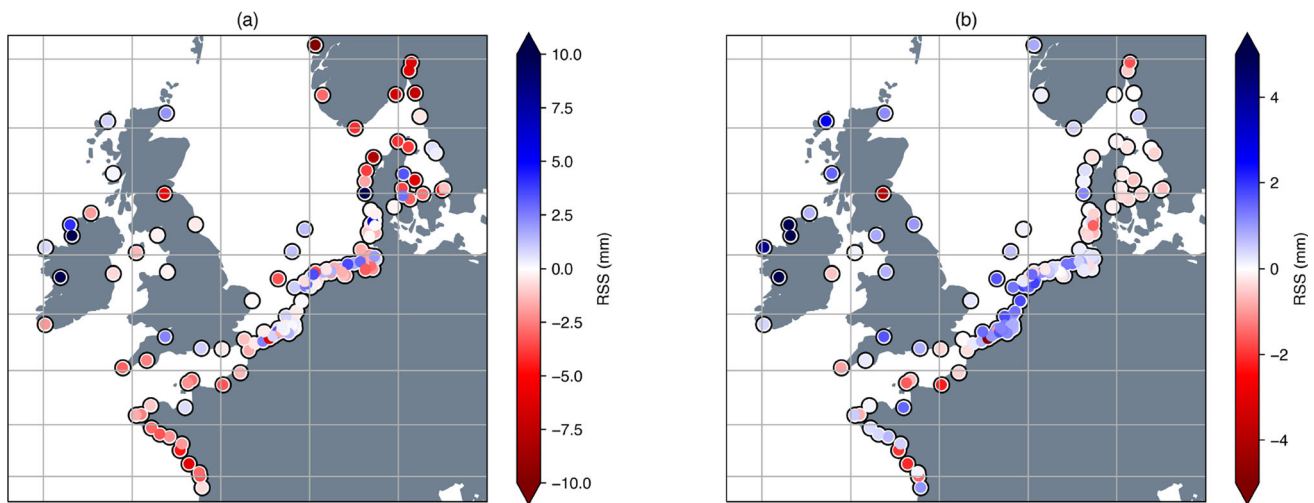


Fig. 10 The RSS difference of all the tidal constituents between the 3D-DCSM-REF and 3D-DCSM-EOT simulations. (a) is the RSS difference with all tides included in the results, and (b) is without the SA tide included

Fig. 10b, the SA has been removed from the RSS estimations to give a better illustration of the influence the other constituents have on the results of the model. Particularly, the S1, RHO1, M6, MA2, MKS2 and MB2 tidal constituents all showed improvements when incorporated from EOT-NECS. Table 2 shows the tides that had the biggest change in the 3D model, with a restriction being only tides that have exceeded a 0.5 mm change in RMS values. Although the changes made to the overall tidal height and total water levels are considerably smaller compared to those seen in the 2D model, there remains a benefit in the model when forcing at the boundaries using the EOT-NECS model. Of particular value are the tides that were originally tested in DCSM-B and DCSM-C, which were originally identified as constituents which would benefit the most from as a boundary forcing from EOT-NECS, which all show to have the largest positive impact on the model. These findings and the negative impact seen by the SA tide demonstrate the significance of these studies to evaluate individual constituent influences in refining the overall tidal and total water height estimations.

4.4 The major tides

A clear omission from the above experiments is the major tidal constituents, which have been shown to be strongly improved in EOT-NECS with respect to EOT20 (Fig. 4). Initial experiments did test the incorporation of these major tides from both EOT20 and EOT-NECS at the boundaries of DCSM-FM. These constituents are originally provided by the FES2014 (O1, Q1, P1, S2) and the GTSMv4.1 (M2, N2, K1, K2) models respectively. In the simulation comparing these tides from EOT-NECS, these tides had negligible impacts on the overall results of the DCSM-FM configuration, with an

overall mean RMS degradation of 0.02 mm when using these tides from EOT-NECS. This is expected as at the boundaries, the four tides taken from FES2014 and the tides taken from EOT-NECS show negligible differences.

Furthermore, the hydrodynamic model, GTSMv4.1, used for the other four major constituents, is calibrated using some of the tide gauges used in the validation of DCSM-FM along the Dutch coastline. Therefore, when coupling this calibration with the accuracy of GTSMv4.1 in this region as well as its high spatial resolution along the European shelf region ($1/90^\circ$) (Wang et al. 2022), it is expected that the major tides from GTSMv4.1 provide suitable boundary forcings for DCSM-FM. From the initial experiments comparing these major tides from either GTSMv4.1, FES2014 or EOT-NECS, this was the case (not shown). It is important to emphasise that the chosen tides for the above experiments were based on constituents that were highly erroneous within DCSM-FM and, therefore, would be of the greatest benefit in terms of improvements possible within DCSM-FM. However, avenues of merging the EOT-NECS and GTSMv4.1 based either on residual tidal analysis or a combination through machine learning or super-resolution (Barthélémey et al. 2022) begin to emerge to benefit from the performance of both of these models in this region. This is not the subject of this manuscript but will be investigated further in future studies.

5 Conclusion

This paper aimed to address two main points: (1) to develop an improved high-resolution EOT model and (2) to improve the representation of tides and water levels within DCSM-FM. Firstly, this involved the development and production of

a regional version of the empirical ocean tide model, EOT-NECS, which was designed to improve on the predecessor global configuration, EOT20, by making some model refinements as well as by including additional satellite altimetry missions to help improve the models' spatial resolution and allow for the estimation of additional tidal constituents. Analysis of the models' performance against in situ observations taken from the updated TICON-3 (Hart-Davis et al. 2022b) showed an improvement compared to the global EOT20 model of 0.678 cm for the eight major tidal constituents and showed a reduced RMS for all tidal constituents. These results allow for the conclusion that the new regional version of the model outperforms the global configuration in the North European Continental Sea region.

This has two positive implications, one being that this new EOT-NECS model should be preferred for applications within this region. Several applications such as the one in this paper but also regional altimetry-based applications (e.g. Birol et al. 2017; Rulent et al. 2020; Dettmering et al. 2021; Passaro et al. 2021) would also benefit from the regional improvements made to tidal estimations. These applications may also be supported by the incorporation of additional tidal constituents. Secondly, there is a potential that the model configuration will perform well in other regions, which opens the door for additional regional versions of the model. Evaluating the model in more regions is also essential in support of ongoing developments with future iterations of the global EOT model in mind.

Once developed, several experiments were designed to test the use of tidal constituents from EOT-NECS as boundary forcings for DCSM-FM. These experiments demonstrated positive implications on DCSM-FM based on the inclusion of most tidal constituents replaced or included from EOT-NECS. The experiments incorporating the S1, MA2, MB2 and RHO1 constituents resulted in mean reductions in the error of these individual constituents as well as the total tidal height and water levels within DCSM-FM. Thanks to the development of the regional configuration, MA2, MB2 and RHO1 constituents were estimated for the first time within EOT-NECS and forced at the boundary of DCSM-FM. For the S1 tide, previously taken from FES2014, an improvement was seen in including this tide from EOT-NECS. This is likely due to FES2014's S1 originating mostly from the atmospheric forcing (Lyard et al. 2021), which, due to DCSM-FM introducing the inverse barometer correction at the boundary, likely produces a double counting of diurnal variations in the air pressure, which is not the case when using the EOT-NECS S1 tide. The NU2, MU2, and M8 tidal constituents were the only added tides that showed a reduction in accuracy with DCSM-FM. In Hart-Davis et al. (2021b), in three different regions, it was concluded that the MU2 and NU2 tides should

not be directly estimated from empirical models, and different techniques should be explored to include these tides in experiments. This study supports these findings and adds that despite making improvements to tidal estimations within the EOT-NECS model, these tides should still not be directly estimated, and in this case, taking these tides from FES2014 should be preferred.

The total changes made to the tidal boundary forcing of the DCSM-FM by incorporating the EOT-NECS tidal constituents had an overall positive impact on the model results. In total, the mean improvement was 0.29 cm in RMS for the tidal height and 0.25 cm for total water level when comparing the reference model with the final version, while in some regions, such as the French and the UK coastlines, there were reductions in RMS exceeding 1 cm. Considering that tides along the coastline are known to have errors relating to individual constituents exceeding 4 cm from global tide models (Stammer et al. 2014), this reduction is considerable in providing accurate water level estimations.

Furthermore, when putting into context that the constituents presented in this study are deemed 'minor' tides, having a considerably smaller influence on the overall tidal height estimation, these improvements are important. For the major tides, there are clear benefits in continuing to utilise the already calibrated GTSMv4.1 model in the DCSM-FM; however, potential future work based on the results seen in this study could involve developing techniques to merge the benefits of the EOT-NECS and GTSM models using either residual tidal analysis or machine learning techniques such as super-resolution (Barthélémy et al. 2022).

Although not the main focus of this study, the impacts on the 3D DCSM-FM estimated water levels and tides were also assessed. The total tidal height and total water level differences when including EOT-NECS constituents were negligible. The RSS estimation of the tidal constituents was negatively impacted by the inclusion of the SA tide, but when this tide was removed, the inclusion of EOT-NECS had positive impacts throughout the domain. This demonstrates a clear benefit based on individual constituent performances of including these tides within the 3D version of the model. The individually improved tides also correlate well with those tested in the 2D experiments, which further emphasises the importance of their inclusion, particularly due to the 3D model incorporating additional processes not included in the 2D model, such as baroclinic processes. It is clear that the SA tide requires special attention, and this will be done in future studies by attempting to remove the mesoscale variability from the SLA data used to derive the tidal constituents, so as not to double count for these effects within the 3D DCSM-FM, following techniques such as those presented in Zaron and Ray (2018) and Bonaduce et al. (2021).

This paper finally highlights the importance of testing different ocean tide models as boundary forcing for numerical models. It is expected that certain tide models perform better in different regions based on refinements made to processing techniques, spatial resolutions etc., so it is worth it to evaluate multiple when producing numerical model simulations that would benefit from tidal forcing along the boundary. Furthermore, a potential future study that could be conducted by the tide modelling community is to produce a comparison of ocean tide models from a spatial perspective to conclude on recommended tide models for applications in particular regions which would make it easier in applications like the above, as well as in the context of tidal correction for satellite altimetry, to decide on which tide model(s) are appropriate for particular applications.

Appendix A

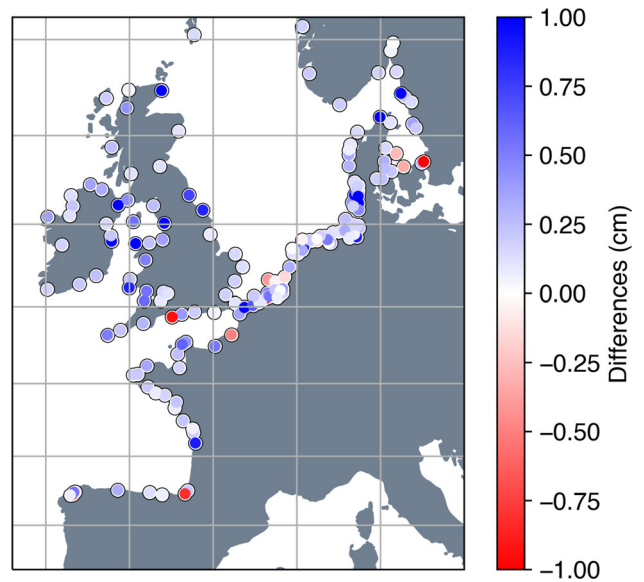


Fig. 12 The RSS differences between DCSM-D minus DCSM-C with the MU2 and NU2 tidal constituents being removed

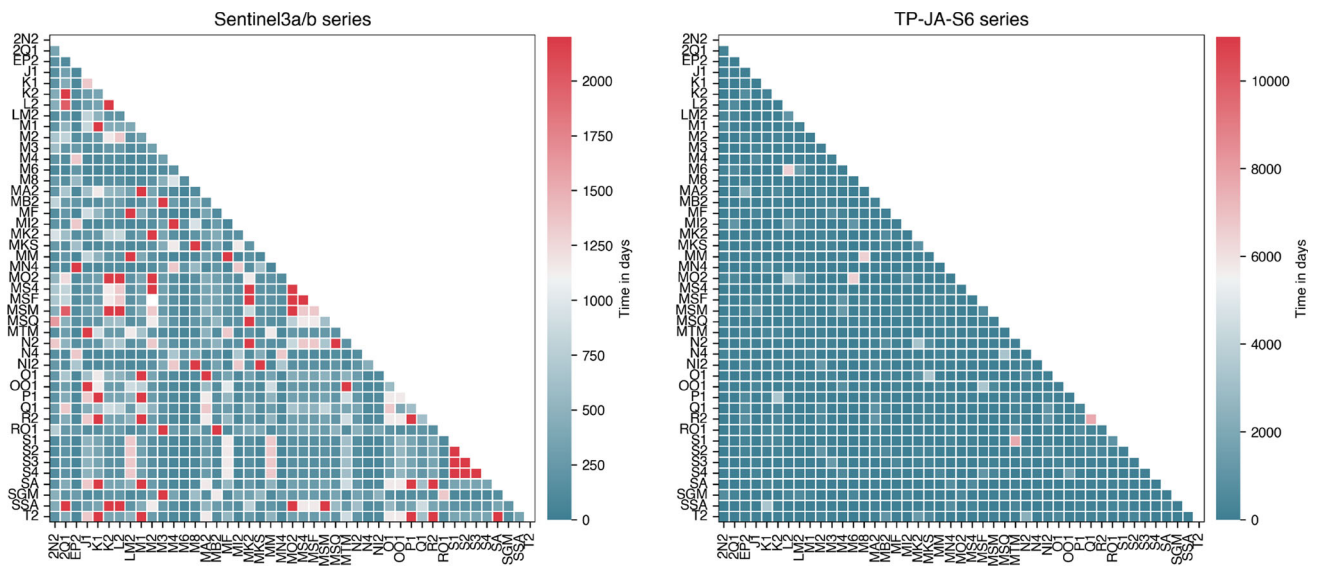


Fig. 11 Rayleigh coefficient of Sentinel3a/b and the TP-JA-S6 orbits

Table 2 RMS difference between the 3D model version of the tidal constituents that have an equal or exceed a difference of 0.5 mm

Constituent	RMS (mm)
SA	7.08
RHO1	−1.84
S1	−1.72
M6	−1.18
H2	−0.78
LABDA2	0.68
MKS2	−0.60
H1	−0.50

Positive values display an increased RMS when the particular EOT-NECS tide is included, and negative values mean a reduced RMS

Acknowledgements The authors acknowledge the DFG project TIDUS-2 (DE2174/12-2, Project Number 388296632) within the DFG research unit NEROGRAV (RU 2736), which partly funds this study.

Data Availability The EOT-NECS data is available at SEANOE: <https://doi.org/10.17882/94705/> (Hart-Davis et al. 2023). EOT20 can be downloaded here: <https://doi.org/10.17882/79489>. The satellite altimetry data used in this study is a modified version of that available from <https://openadb.dgfi.tum.de/en/>, and the GESLA-3 data used in the creation of TICON-3 is available at <https://www.gesla.org/>. The TICON-3 dataset is available at <https://doi.pangaea.de/10.1594/PANGAEA.951610>

Declarations

Conflict of interest The authors declare no competing interests.

Open Access This article is licensed under a Creative Commons Attribution 4.0 International License, which permits use, sharing, adaptation, distribution and reproduction in any medium or format, as long as you give appropriate credit to the original author(s) and the source, provide a link to the Creative Commons licence, and indicate if changes were made. The images or other third party material in this article are included in the article's Creative Commons licence, unless indicated otherwise in a credit line to the material. If material is not included in the article's Creative Commons licence and your intended use is not permitted by statutory regulation or exceeds the permitted use, you will need to obtain permission directly from the copyright holder. To view a copy of this licence, visit <http://creativecommons.org/licenses/by/4.0/>.

References

- Andersen OB (1995) Global ocean tides from ERS 1 and TOPEX/POSEIDON altimetry. *J Geophys Res* 100(C12):25–249. <https://doi.org/10.1029/95jc01389>
- Arns A, Dangendorf S, Jensen J, et al (2017) Sea-level rise induced amplification of coastal protection design heights. *Sci Reports* 7(1). <https://doi.org/10.1038/srep40171>
- Barthélémy S, Brajard J, Bertino L et al (2022) Super-resolution data assimilation. *Ocean Dyn* 72(8):661–678. <https://doi.org/10.1007/s10236-022-01523-x>
- Birol F, Fuller N, Lyard F et al (2017) Coastal applications from nadir altimetry: example of the X-TRACK regional products. *Adv Space Res* 59(4):936–953. <https://doi.org/10.1016/j.asr.2016.11.005> <https://www.sciencedirect.com/science/article/pii/S0273117716306317>
- Bonaduce A, Cipollone A, Johannessen JA et al (2021) Ocean mesoscale variability: a case study on the Mediterranean Sea from a re-analysis perspective. *Front Earth Sci* 9. <https://doi.org/10.3389/feart.2021.724879>
- Bosch W, Dettmering D, Schwatke C (2014) Multi-mission cross-calibration of satellite altimeters: constructing a long-term data record for global and regional sea level change studies. *Remote Sens* 6(3):2255–2281. <https://doi.org/10.3390/rs6032255> <https://www.mdpi.com/2072-4292/6/3/2255>
- Bähr H, Altamimi Z, Heck B (2007) Variance component estimation for combination of terrestrial reference frames. *Tech. Rep. 6*, Karlsruher Institut für Technologie (KIT), <https://doi.org/10.5445/KSP/1000007363>
- Cartwright DE (1999) *Tides : a scientific history* / David Edgar Cartwright. Cambridge University Press, Cambridge, UK
- Cartwright DE, Ray RD (1991) Energetics of global ocean tides from Geosat altimetry. *J Geophys Res Oceans* 96(C9):16897–16912. <https://doi.org/10.1029/91JC01059> <https://agupubs.onlinelibrary.wiley.com/doi/abs/10.1029/91JC01059> <https://arxiv.org/abs/agupubs.onlinelibrary.wiley.com/doi/pdf/10.1029/91JC01059>
- Cheng Y, Andersen OB (2017) Towards further improving DTU global ocean tide model in shallow waters and Polar Seas. In OSTST, Poster in: Proceedings of the Ocean Surface Topography Science Team (OSTST) Meeting, Miami FL USA, pp 23–27. https://ftp.space.dtu.dk/pub/DTU16/OCEAN_TIDE/OSTST2017-tide.pdf
- Cipollini P, Benveniste J, Birol F, et al (2017) Satellite altimetry in coastal regions. In *Satellite Altimetry over Oceans and Land Surfaces*. CRC Press, p 343–380. <https://doi.org/10.1201/9781315151779-11>
- Darwin GH (1891) XI. on the harmonic analysis of tidal observations of high and low water. *Proc R Soc Lond* 48(292–295):278–340. <https://doi.org/10.1098/rsp1.1890.0041>
- Dettmering D, Müller FL, Oelmann J et al (2021) North SEAL: a new dataset of sea level changes in the North Sea from satellite altimetry. *Earth Syst Sci Data* 13(8):3733–3753. <https://doi.org/10.5194/essd-13-3733-2021> <https://essd.copernicus.org/articles/13/3733/2021/>
- Egbert GD, Ray RD (2003) Semi-diurnal and diurnal tidal dissipation from TOPEX/Poseidon altimetry. *Geophys Res Lett* 30(17). <https://doi.org/10.1029/2003GL017676> <https://agupubs.onlinelibrary.wiley.com/doi/abs/10.1029/2003GL017676> <https://arxiv.org/abs/https://agupubs.onlinelibrary.wiley.com/doi/pdf/10.1029/2003GL017676>
- Egbert GD, Ray RD (2017) Tidal prediction. *J Mar Res* 75(3):189–237. <https://doi.org/10.1357/002224017821836761>
- EMODnet Bathymetry Consortium (2020) EMODnet digital bathymetry (DTM 2020). <https://doi.org/10.12770/bb6a87dd-e579-4036-abe1-e649cea9881a>
- Goede EDD (2020) Historical overview of 2D and 3D hydrodynamic modelling of shallow water flows in the Netherlands. *Ocean Dynamics* 70(4):521–539. <https://doi.org/10.1007/s10236-019-01336-5>
- Hackett B, Donnelly C, Sagarminaga Y (2013) Deliverable 4.1 report on validation of E-HYPE runoff data. https://www.researchgate.net/publication/259146801_Report_on_validation_of_E-HYPE_runoff_data
- Haigh ID, Marcos M, Talke SA, et al (2022) GESLA Version 3: a major update to the global higher-frequency sea-level dataset. *Geoscience Data Journal* n/a(n/a). <https://doi.org/10.1002/gdj3.174> <https://rmets.onlinelibrary.wiley.com/doi/abs/10.1002/gdj3.174>

- 174 <https://arxiv.org/abs/https://rmets.onlinelibrary.wiley.com/doi/pdf/10.1002/gdj3.174>
- Hart-Davis M, Dettmering D, Sulzbach R et al (2021) Regional evaluation of minor tidal constituents for improved estimation of ocean tides. *Remote Sens* 13(16):3310. <https://doi.org/10.3390/rs13163310> <https://www.mdpi.com/2072-4292/13/16/3310>
- Hart-Davis MG, Piccioni G, Dettmering D et al (2021) EOT20: a global ocean tide model from multi-mission satellite altimetry. *Earth Syst Sci Data* 13(8):3869–3884. <https://doi.org/10.5194/essd-13-3869-2021> <https://essd.copernicus.org/articles/13/3869/2021/>
- Hart-Davis MG, Dettmering D, Seitz F (2022a) TICON-3: tidal constants based on GESLA-3 sea-level records from globally distributed tide gauges including gauge type information (data). <https://doi.pangaea.de/10.1594/PANGAEA.951610>
- Hart-Davis MG, Dettmering D, Seitz F (2022b) TICON: tidal constants. <https://doi.org/10.1594/PANGAEA.946889>
- Hart-Davis MG, Schwatke C, Dettmering D, et al (2023) EOT-NECS Ocean Tide Model. <https://doi.org/10.17882/94705>
- Hersbach H, Bell B, Berrisford P, et al (2017) Complete ERA5 from 1979: fifth generation of ECMWF atmospheric reanalyses of the global climate. Copernicus Climate Change Service (C3S) Data Store (CDS), ECMWF [data set]
- Intergovernmental Panel on Climate Change (IPCC) (2022) Changing ocean, marine ecosystems, and dependent communities. <https://doi.org/10.1017/9781009157964.007>
- Kernkamp H, van Dam A, Stelling G et al (2011) Efficient scheme for the shallow water equations on unstructured grids with application to the continental shelf. *Ocean Dyn Theor Comput Oceanogr Monit* 61(8):1175–1188. <https://doi.org/10.1007/s10236-011-0423-6>
- Lyard FH, Allain DJ, Cancet M et al (2021) FES 2014 global ocean tide atlas: design and performance. *Ocean Sci* 17(3):615–649. <https://doi.org/10.5194/os-17-615-2021>
- Muis S, Verlaan M, Winsemius HC, et al. (2016) A global reanalysis of storm surges and extreme sea levels. *Nature Commun* 7(1). <https://doi.org/10.1038/ncomms11969>
- Passaro M, Cipollini P, Vignudelli S et al (2014) ALES: a multi-mission adaptive subwaveform retracker for coastal and open ocean altimetry. *Remote Sens Environ* 145:173–189. <https://doi.org/10.1016/j.rse.2014.02.008> <https://www.sciencedirect.com/science/article/pii/S0034425714000534>
- Passaro M, Müller FL, Oelmann J et al (2021) Absolute Baltic Sea level trends in the satellite altimetry era: a revisit. *Front Mar Sci* 8:546. <https://doi.org/10.3389/fmars.2021.647607>
- Piccioni G, Dettmering D, Bosch W et al (2019) TICON: tidal constants based on GESLA sea-level records from globally located tide gauges. *Geosci Data J* 6(2):97–104. <https://doi.org/10.1002/gdj3.72>
- Prandi P, Meyssignac B, Ablain M, et al. (2021) Local sea level trends, accelerations and uncertainties over 1993–2019. *Sci Data* 8(1). <https://doi.org/10.1038/s41597-020-00786-7>
- Provost CL, Bennett AF, Cartwright DE (1995) Ocean tides for and from TOPEX/POSEIDON. *Science* 267(5198):639–642. <https://doi.org/10.1126/science.267.5198.639>
- Pugh DT (1987) Tides, surges and mean sea level. John Wiley and Sons <https://www.osti.gov/biblio/5061261>
- Ray RD (2017) On tidal inference in the diurnal band. *J Atmos Ocean Technol* 34(2):437–446. <https://doi.org/10.1175/JTECH-D-16-0142.1> <https://journals.ametsoc.org/view/journals/atot/34/2/jtech-d-16-0142.1.xml>
- Ray RD (2022) Technical note: on seasonal variability of the m_2 tide. *Ocean Sci* 18(4):1073–1079. <https://doi.org/10.5194/os-18-1073-2022> <https://os.copernicus.org/articles/18/1073/2022/>
- Rulert J, Calafat FM, Banks CJ et al (2020) Comparing water level estimation in coastal and shelf seas from satellite altimetry and numerical models. *Front Mar Sci* 7. <https://doi.org/10.3389/fmars.2020.549467> <https://www.frontiersin.org/articles/10.3389/fmars.2020.549467>
- Savcenko R, Bosch W (2012) EOT11a-empirical ocean tide model from multi-mission satellite altimetry. DGFI Report No 89 <https://doi.org/10.1594/PANGAEA.834232>
- Smith AJE (1999) Application of satellite altimetry for global ocean tide modeling. TU Delft. <http://resolver.tudelft.nl/uuid:5e9c5527-220f-4658-b516-459528e62733>
- Stammer D, Ray RD, Andersen OB et al (2014) Accuracy assessment of global barotropic ocean tide models. *Rev Geophys* 52(3):243–282. <https://doi.org/10.1002/2014RG000450> <https://agupubs.onlinelibrary.wiley.com/doi/abs/10.1002/2014RG000450> <https://arxiv.org/abs/agupubs.onlinelibrary.wiley.com/doi/pdf/10.1002/2014RG000450>
- van de Wal RSW, Zhang X, Minobe S et al (2019) Uncertainties in long-term twenty-first century process-based coastal sea-level projections. *Surv Geophys* 40(6):1655–1671. <https://doi.org/10.1007/s10712-019-09575-3>
- Wang X, Verlaan M, Veenstra J et al (2022) Data-assimilation-based parameter estimation of bathymetry and bottom friction coefficient to improve coastal accuracy in a global tide model. *Ocean Sci* 18(3):881–904. <https://doi.org/10.5194/os-18-881-2022> <https://os.copernicus.org/articles/18/881/2022/>
- Woodworth PL, Green JAM, Ray RD et al (2021) Preface: Developments in the science and history of tides. *Ocean Sci* 17(3):809–818. <https://doi.org/10.5194/os-17-809-2021> <https://os.copernicus.org/articles/17/809/2021/>
- Zaron ED, Ray RD (2018) Aliased tidal variability in mesoscale sea level anomaly maps. *J Atmos Ocean Technol* 35(12):2421–2435. <https://doi.org/10.1175/jtech-d-18-0089.1>
- Zijl F, Groenenboom J (2019) Development of a sixth generation model for the NW European Shelf (DCSM-FM 0.5nm). Tech rep, Deltares, Deltares
- Zijl F, Verlaan M, Gerritsen H (2013) Improved water-level forecasting for the Northwest European Shelf and North Sea through direct modelling of tide, surge and non-linear interaction. *Ocean Dyn* 63(7):823–847. <https://doi.org/10.1007/s10236-013-0624-2>
- Zijl F, Verlaan M, Sumihar J (2015) Application of data assimilation for improved operational water level forecasting on the Northwest European Shelf and North Sea. *Ocean Dyn* 65(12):1699–1716. <https://doi.org/10.1007/s10236-015-0898-7>